ARTICLE

Check for updates

Bi-allelic variants in human *TCTE1/DRC5* cause asthenospermia and male infertility

Shushu Zhou[1,5], Huan Wu[2,3,5], Jintao Zhang[1,5], Xiaojin He[2,3], Siyu Liu[1], Ping Zhou[2,3], Rong Hua[2,3,4]✉, Yunxia Cao[2,3,4]✉ and Mingxi Liu[1]✉

Asthenozoospermia (AZS) is a common male infertility phenotype, accounting for 18% of infertile patients. The N-DRC (Nexin-dynein Regulatory Complex) complex is the motor regulating device in the flagellum, which is found in most eukaryotic organisms with flagellum. The deletion of TCTE1 (T-Complex-Associated Testis-Expressed 1), a component of the N-DRC complex also known as DRC5 (Dynein regulatory complex subunit 5), has been shown to cause asthenospermia in mice. This study mainly introduces a clinical case of male infertility with normal sperm count, normal morphological structure, but low motility and weak forward movement. By whole-exome sequencing, we found that *TCTE1* became a frameshift mutant, ENST00000371505.5: c.396_397insTC (p.Arg133Serfs*33), resulting in the rapid degradation of TCTE1 protein and male infertility. This phenotype is similar to the *Tcte1*$^{-/-}$ (*Tcte1* knockout) mice, which showed structural integrity but reduced motility. Further, different from mice, in vitro Fertilization (IVF) could successfully solve the patient's problem of infertility. Our data provides a better understanding of the biological functions of TCTE1 in human flagellum assembly and male fertility.

European Journal of Human Genetics (2022) 30:721–729; https://doi.org/10.1038/s41431-022-01095-w

INTRODUCTION

Asthenospermia (AZS) is a broadly defined condition of low sperm motility, wherein the forward sperm motility is <32% or the total motility is <40%. Interestingly, in most cases of dysfunctional sperm motility, the phenotype is not entirely asthenozoospermic, but is a combination of AZS and oligo- and/or teratozoospermia [1]. Therefore, along with low sperm motility, numerous anatomical aberrations are usually evident in the sperm flagella [2–18]. In the early study of AZS cases, nearly a quarter of the AZS patients (about 18.71%) displayed no apparent structural defects in the sperm axoneme [1, 19]. For instance, the *SPAG17* deficient sperm exhibited a complete lack of mobility. However, apart from the absence of its own central pair complex (CPC), no obvious anomalies was detected in the sperm morphology under optical microscope, therefore, establishing a pure AZS phenotype [20]. In addition, some genetic defects, such as, *DNAH5*, *CCDC40*, *RSPH9*, *ARL2BP*, and so on produce syndromic AZS, with an assortment of concurrent clinical symptoms [21–24].

The N-DRC complex is a structural hub located between two groups of doublet microtubules, dynein arms, and radial spoke on the axoneme of cilia and flagellum, and it regulates beating of the cilia and flagellum [25, 26]. TCTE1 (T-Complex-Associated Testis-Expressed 1), also known as DRC5 (Dynein regulatory complex subunit 5), is a subcomponent of N-DRC.

Thus far, *Tcte1* was only reported in mice, and its deficiency was shown to cause male infertility. Spermatozoa from *Tcte1*$^{-/-}$ mice exhibited decreased motility and poor forward movement. Moreover, although *Tcte1*$^{-/-}$ sperm flagella function was abrogated, flagellum ultrastructure remained normal [27]. This study suggests that loss of TCTE1 may lead to a purely AZS phenotype in male mice. However, whether TCTE1 deletion affects the N-DRC complex and whether this deletion affects human sterility and how to restore this condition remained a mystery.

Using whole exome sequencing (WES) as a clinical genetic diagnostic, we were the first to identify a patient with a pathological homozygous variant in the *TCTE1* gene. Moreover, unlike mice, we demonstrated that IVF can be successfully used to solve the infertility problem of TCTE1-deficient sperm, suggesting the possibility of functional differences in the human and mice sperms.

MATERIALS AND METHODS

Human specimen

Human sperm sample were acquired from the First Affiliated Hospital of Anhui Medical University. The patient diagnosis was as follows: primary infertility with AZS. Karyotypic analyses of the patient was normal (46, XY), as were hormone levels, bilateral testicular size distributions, and secondary sex characteristics. This patient provided informed consent to participate, and the study was in accordance with the Declaration of Helsinki.

[1]State Key Laboratory of Reproductive Medicine, Department of Histology and Embryology, School of Basic Medical Sciences, Nanjing Medical University, Nanjing 211166, China. [2]Reproductive Medicine Center, Department of Obstetrics and Gynecology, the First Affiliated Hospital of Anhui Medical University, Hefei 230022, China. [3]NHC Key Laboratory of Study on Abnormal Gametes and Reproductive Tract (Anhui Medical University), Hefei 230032, China. [4]Key Laboratory of Population Health Across Life Cycle (Anhui Medical University), Ministry of Education of the People's Republic of China, Hefei 230032, China. [5]These authors contributed equally: Shushu Zhou, Huan Wu, Jintao Zhang.
✉email: ahmuhuarong@126.com; caoyunxia6@126.com; mingxi.liu@njmu.edu.cn

Received: 14 October 2021 Revised: 15 March 2022 Accepted: 21 March 2022
Published online: 7 April 2022

WES
130 patients with abnormal sperm motility were recruited, including 88 patients with multiple morphological abnormalities of the sperm flagella (MMAF) and 42 patients with asthenospermia. WES was conducted for the enrolled patients using gDNA isolated from peripheral blood via a DNeasy Blood and Tissue kit (QIAGEN). An Agilent SureSelectXT Human All Exon Kit was utilized to isolate and enrich exonic sequences, following which the samples were sequenced on the Illumina HiSeq X-TEN platform. Standard assembly (Burrows–Wheeler Aligner), calling (Genome Analysis Toolkit), and annotation (ANNOVAR) were then performed as part of the sequencing analyses, as detailed previously [14].

Animals
The mice were maintained in standard animal housing (20–22 °C; 50–70% humidity; 12 h light/dark cycle) with open access to food and water. The Institutional Animal Care and Use Committees of Nanjing Medical University provided approval for this study (Approval No. IACUC-2004020), and all animal protocols abided by the Care and Use of Laboratory Animals and institutional guidelines.

Antibodies
Rabbit anti-RSPH9 (23253-1-AP) was obtained from Proteintech (Wuhan, China). Mice anti-β-Tubulin (AC021) was from Abclonal (Wuhan, China). Rabbit anti-Acetylated Tubulin was purchased from Cell Signaling Technology (MA, USA). Lastly, mice anti-Acetylated Tubulin (T6793) was from Sigma-Aldrich. Antibodies targeting DRC1, DRC2, DRC3, DRC4, TCTE1, and DRC7 were prepared as per prior published protocols [28]. Briefly, mice DRC1 (aa 1-146), CCDC65/DRC2 (aa 1-126), DRC3 (aa 182-300), GAS8/DRC4 (aa 1-478), TCTE1/DRC5 (aa 334-498), and DRC7 (aa 1-292) were expressed as His fusion proteins in *E. coli*, using the pET-28a (+) vector. Subsequently, the Ni-NTA His Bind Resin was used to affinity purify these proteins, before immunization of the resultant fusion proteins, yielding the six following antiserum preparations: anti-DRC1, anti-DRC2, anti-DRC3, anti-DRC4, anti-DRC5, and anti-DRC7.

Cell strains
HEK293T cell strains were obtained from ATCC and cultured in a 37°C cell incubator.

Plasmid
The original pCAG plasmid was a gift from the Ikawa laboratory, Osaka University [29]. Based on the original plasmid, we constructed a WT plasmid with human *TCTE1* CDS sequence and a flag tag. The MUT plasmid was generated via insertion of TC bases in between the 396 and 397 bases of the *TCTE1* CDS sequence of WT plasmid.

Tcte1 mutant mice generation
The establishment of the *Tcte1* mutant mice model was as previously reported (Castaneda, et al., [27]).

H&E staining
Paraffin embedded tissue sections were first dewaxed in xylene, then received staining, and hydration from 100% alcohol to 70% alcohol, with 2 min incubations in each step, before being submerged in double distilled water. Hematoxylin (Servicebio) staining was done for 1 min with shaking in 10% HCl to remove excess hematoxylin from the tissue surface, prior to washing with tap water for 10 min. Alcohol soluble eosin (Servicebio) staining was performed for 2–3 min, with subsequent immersion in 100% alcohol for 2 min, and two times exposure to xylene for 15 min each, before resin (Sangon) sealing.

Western blotting
A lysis buffer (50 mM Tris-HCl pH 8.2, 75 Mm NaCl, 8 M urea) with 1x Complete™ EDTA-free Protease Inhibitor Cocktail (Roche, Basel, Switzerland) was employed for protein isolation. The resulting proteins were separated on SDS-PAGE, transferred to PVDF membranes, blocked in 5% non-fat milk in TBS at room temperature (RT) for 2 h, kept overnight (ON) in relevant primary antibodies (PAb) at 4 °C, rinsed with TBST, and exposed to corresponding secondary antibodies (SAb) for 2 h at RT, before protein visualization with the High-sig ECL Western Blotting Substrate (Tanon, Shanghai, China).

Immunofluorescence
Spermatozoa samples were PBS-rinsed three times (10 min/wash), and placed in a microwave oven in 10 mM citrate buffer (pH 6.0) for 10 min to recover antigen. Following three additional PBS washes, the slides were blocked with 5% BSA for 2 h, before ON staining with relevant PAb at 4 °C. Following SAb staining for 2 h at RT, the slides were exposed to Hoechst 33342 counterstaining for 5 min, before PBS-rinse and mounting with glycerol prior to imaging with an LSM800 confocal microscope (Carl Zeiss AG) or a TCS SP8X confocal microscope (Leica Microsystems).

Cycloheximide test
Cycloheximide (Sigma-Aldrich) was introduced 12 h after cell transfection and fluid change. The cells in the 0 min groups were immediately harvested, and the cocktail protease inhibitor (Thermo Scientific) was added. Cells in the second group were harvested 15 min after dosing, and those in the third group were harvested 30 min after dosing. Next, total proteins were extracted for follow-up experiments.

Superovulation (SO) and IVF
To induce SO, female mice (21–23 days old) were intraperitoneally administered with 5 IU of pregnant mare's serum gonadotropin (PMSG) (Ningbo Sansheng Pharmaceutical Corporation, Zhejiang, China). Following a 44 h incubation period, the mice were given 5 IU of human chorionic gonadotropin (HCG) (Ningbo Sansheng Pharmaceutical Corporation, Zhejiang, China). After 14 h, the resulting eggs were harvested from the SO females and maintained in 150 μL of HTF medium under a thin layer of paraffin oil. Meanwhile, epididymal sperms were harvested from 3-mo-old male mice and kept in HTF (AIBI Bio-Technology Co.Nanjing, China) medium for 40 min to induce capacitation. Next, 2 × 105 sperm/ml capacitated sperms were introduced to eggs and incubated for 4 h, until the pronuclei became evident. The fertilized eggs were finally blown clean, maintained in KSOM (AIBI Bio-Technology Co.Nanjing, China) medium, and imaged with a Ti2-U microscope (Nikon, Tokyo, Japan).

TEM
Ultrastructural analyses of testes and spermatozoa using TEM were conducted as previously described. [27, 30] To assess microstructural anatomy, tracheal and epididymal specimen were fixed ON in 2.5% glutaraldehyde, with subsequent exposure to 2% OsO4, and then Araldite for embedding purposes. Ultrathin 80 nm sections staining were then

Table 1. Semen data of the patient.

Semen parameters	Patient sample	Normal values
Color	Gray-white	Milk-white, gray-white, yellowwish
Semen volume(ml)	2.4	≥1.5
PH	7.5	7.2–8.5
Sperm concentration (M/ml)	93.5	≥15
Sperm count (M/ml)	224.3	≥39
Progressive motility (%)	17.9	≥32
Total motility (%)	32.6	≥40
Vitality (%)	NA	≥58
Typical forms (%)	NA	≥4
Round cells (M/ml)	1.9	≦5
VCL (μm/s)	46.6	
VSL (μm/s)	20	
VAP (μm/s)	27	
LIN (%)	43.3	
STR (%)	74	
WOB (%)	58.6	

Normal Values based on the World Health Organization, 2015; *M*, Million; *NA*, Not Available; *VCL*, curvilinear velocity; *VSL*, straight line velocity; *VAP*, average path velocity; *LIN*, linearity; *STR*, straightness; *WOB*, wobble.

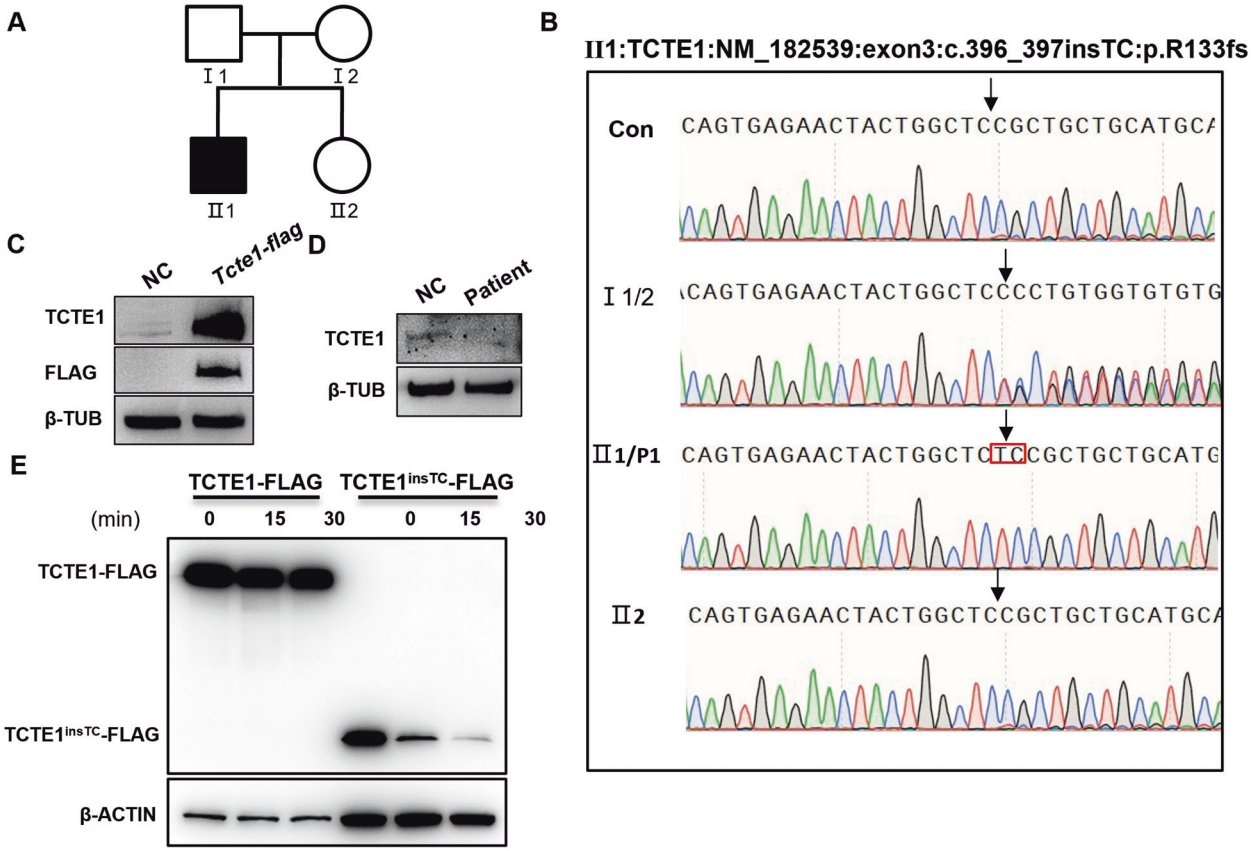

Fig. 1 Schematic representation of the mutated TCTE1 variant and its expression profile. A The sterile patient pedigree. **B** Sanger sequencing confirming the TCTE1 variant, c.396_397ins TC. The proband harbored the homozygous variant. The patient's parents possessed the heterozygous allele, whereas his elder sister carried wild-type alleles. The variant located is represented by a black arrow and the inserted bases are highlighted with a red box. **C** the TCTE1 antibody could specifically identify the overexpressed TCTE1-FLAG fusion protein; β-TUB, β-TUBULIN. **D** TCTE1 is missing in spermatozoa from the patient. **E** Cycloheximide exposure and subsequent Western Blot analysis illustrating the rapid degradation of the truncated TCTE1 protein, expressed by the TCTE1^{TCins}-FLAG vector, in relation to the control TCTE1 protein, expressed by the TCTE1-FLAG vector at time points 0 min, 15 min, and 30 min after dosing.

done with uranyl acetate and lead citrate, and analysis with an electron microscope (JEM.1010, JEOL). Cross sections of more than 30 spermatozoa from 3 discontinuous sections were observed in each sample. The N-DRC structure can always be found in the cross sections with clear microtubules and RS.

RESULT

Basic information and semen analysis of patients

A couple was not pregnant for 5 years after cohabitation without contraception. In 2015, the couple (both 25 years old) was examined in the reproductive medical center of Obstetrics and Gynecology of the First Affiliated Hospital of Anhui Medical University. Upon examination, it was discovered that the husband suffered from primary infertility.

The patient was asked to abstain from sexual intercourse for 3 days prior to the collection of sperm samples via masturbation. These samples were maintained at 37 °C for 30 min to induce liquefaction before dilution, according to the ratio of 1:1, for analysis. The 2015 WHO (World Health Organization) parameters were followed in the collection of semen data. Our analysis revealed that the semen color, smell, pH, and volume from one control ejaculation were normal. Analysis of semen density and motility showed that the sperm density was normal, but the proportion of forward motile sperm was only 17.9%, and the total motility rate was 32.6%, suggesting the existence of the AZS phenotype (Normal range: ≥32%) forward motile sperms or ≥40% total motility rate (WHO, 2015) (Table 1) [31]. Further, Chest X-ray scan was performed and we excluded pulmonary disease and situs inversus in the TCTE1-mutant proband (Figure S1).

WES of patient blood sample uncovered that the patient carried a homozygous frame shift insertion (c.396_397insTC) in the *TCTE1* gene, which likely caused the premature translational arrest of the nascent TCTE1 peptide (p.Arg133Serfs*33). We verified the *TCTE1* variant in the blood samples of the patient and his immediate relatives via Sanger sequencing (Fig. 1A and B).

Due to a lack of sufficient patient sperm protein, we simulated the patient's gene variant and constructed gene expression vectors carrying either the *TCTE1* mutant or a normal genotype for further in vitro cell exploration. Using cycloheximide to block new protein production, we revealed that the mutant *TCTE1* vector produced a truncated protein that degraded faster than the control vector (Fig. 1C). Therefore, we suspected that the AZS of this patient originated from a defect in the *TCTE1* gene. Since sperm analysis showed no abnormality in sperm morphology, IVF was used to make successful fertilization and the couple was able to obtain embryos in vitro (Table 2).

Normal flagellar axoneme structure in the TCTE1 deficient sperm

TCTE1 or DRC5 is one of the structural proteins in the N-DRC complex of *Chlamydomonas* (Fig. 2A), which could cause severe defects in the sperm flagellum [32–34]. To examine the sperm morphology in more detail, we used immunofluorescence

staining to examine the sperm head and axoneme, both of which appeared normal in the TCTE^{R133Sfs*33} and control sperms (Fig. 2B). Next, we compared the TCTE1 deficient sperm with control sperm using Transmission Electron Microscopy (TEM), and found that the TCTE^{R133Sfs*33} sperm exhibited normal "9 + 2" microtubules in the axoneme of sperm tail, along with normal inner and outer dynein arms and spokes, compared to controls. Moreover, the N-DRC could be found between microtubule dublets in the spermatozoa of patient, which is different from the results in the sperm of patients with DRC1 deficiency [35] (Fig. 2C). Given these evidence, TCTE1 deletion did not affect the normal construction of the main structure of the sperm flagellum axoneme. This conclusion is consistent with a previous study on sperms from the *Tcte1*$^{-/-}$ mice [27]. Collectively, although there was no obvious defect in the axoneme structure, TCTE1^{R133Sfs*33} produced an AZS phenotype, marked with low sperm motility and male sterility.

Table 2. IVF data of the patient.

Stage	Counts
Egg	27
MII	13
Zygote	8
Blastocyst	8

TCTE1 deficiency does not affect the expression and localization of basic N-DRC components on the sperm flagellum

The N-DRC complex harbors 11 subunits, including DRC1-11 [25, 36, 37]. Some defects in the DRC component cause local or large N-DRC assembly loss between the two adjacent outer microtubules [25, 38], which may contribute to an abnormal microtubule arrangement and axoneme structure. To clarify the effect of TCTE1 deficiency on N-DRC in human and mice sperm flagellum, we carried out immunofluorescence (human sperm) and western blot (mice sperm) analysis of different DRC proteins within the sperm flagellum. Based on our results, apart from the low DRC5 expression, due to DRC5 deletion, other DRC proteins like DRC1-4 and DRC7 exhibited normal expression and localization within the sperm flagellum, relative to controls (Fig. 3A–G). Hence TCTE1 deletion did not influence the expression and localization of other N-DRC subunits in the flagellum of human and mice sperms.

IVF was successful in impregnating the couple

The reproductive center of the First Affiliated Hospital of Anhui Medical University successfully resolved infertility of the AZS patient, resulting in impregnation of the female partner via IVF. Among the 27 oocytes obtained during IVF, 8 oocytes were fertilized to form 2 PN (two pronucleus), and entered the cleavage phase successfully (Table 2). The couple carried the baby to term and gave birth in 2016, confirming that TCTE1 deficiency can be resolved with IVF technology.

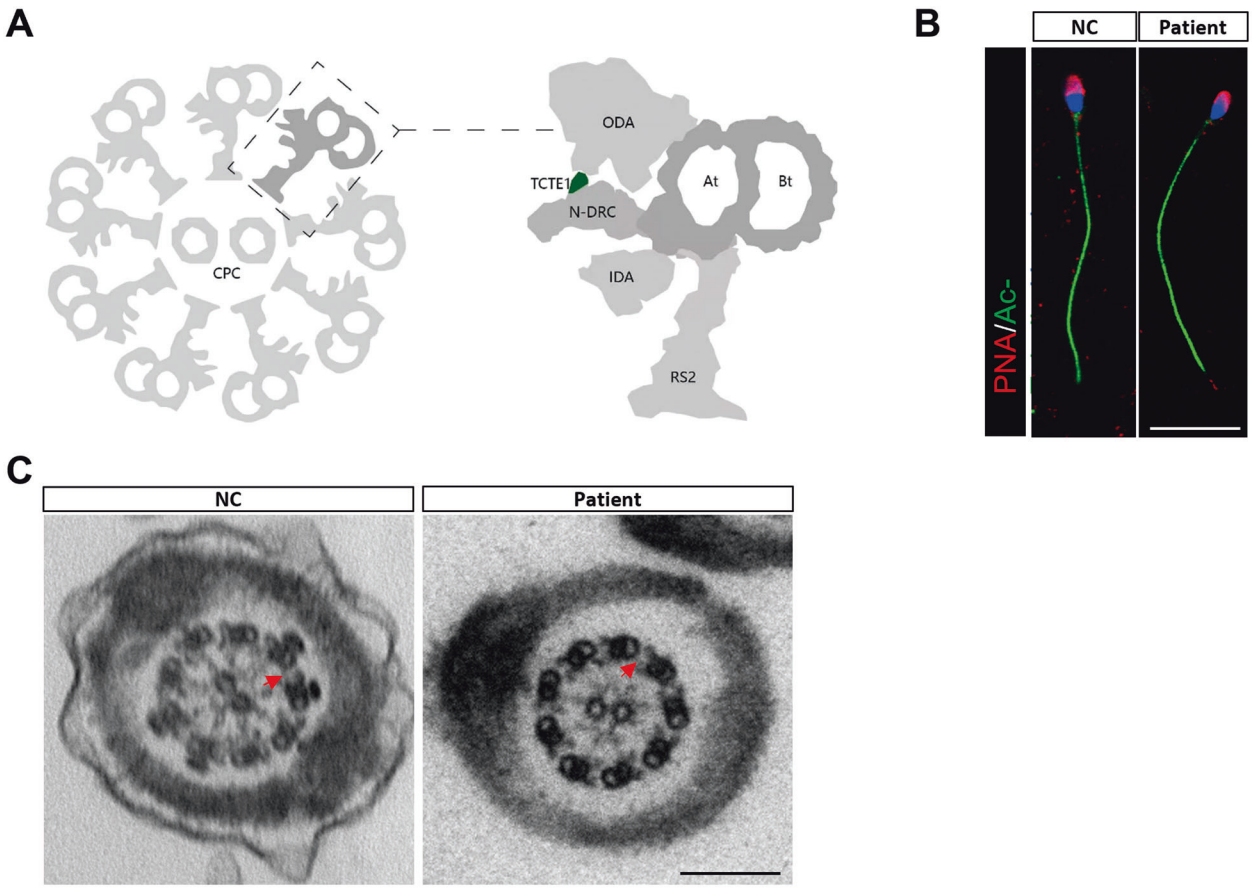

Fig. 2 Morphological observations of the patient sperm using TEM and immunofluorescence. A A cross-sectional model of the axonemal components of the sperm flagellum; N-DRC, nexin-dynein regulatory complex; CPC, central-pair complex; ODA, out dynein arm; IDA, inner dynein arm; At, A-tubule; Bt, B-tubule; Rs2, radial spoke 2. **B** Immunofluorescent evaluation of acetylated-TUBULIN (green), Peanut arachis hypogaea agglutinin (PNA, red), and Hoechst (blue) in control and patient sperms; scale bar = 10 μm. **C** The flagellar cross sectional structure of control human and patient using TEM. The N-DRC complex is represented by a red arrow; scale bar = 200 nm.

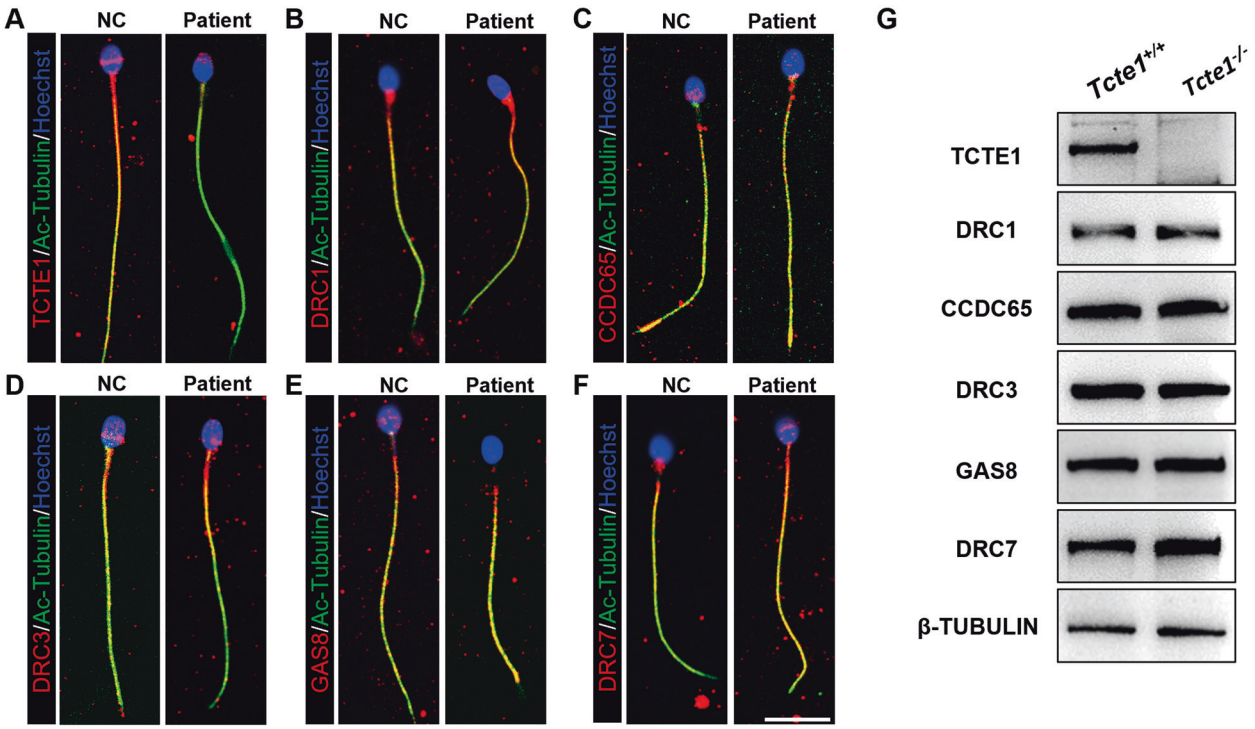

Fig. 3 Expression and localization of N-DRC components in the human and mice sperm flagellum. A–F Immunofluorescence depicting different DRCs' locations on the human sperm flagella. TCTE1/DRC5 was not detected in the patient sample (**A**). However, DRC1 (**B**), CCDC65/DRC2 (**C**), DRC3(D), GAS8/DRC4(**E**), and DRC7 (**F**) were detected. DRCs (red), acetylated-TUBULIN (green), and Hoechst (blue); scale bar = 10 μm. **G** Western Blot evaluation of mice sperm proteins. DRC1, CCDC65/DRC2, DRC3, GAS8/DRC4, and DRC7 were expressed, but not TCTE1/DRC5.

In mice, however, the success of IVF was remarkably low, compared to wild type mice (Fig. 4A, B). In 6 distinct experiments, 726 eggs were subjected to fertilization. But, only 21 eggs were successfully fertilized, among which, only 2 reached the cleavage phase, and developed into blastocysts (Table 3). Using the Bohboh software to assess sperm trajectory movement [39], we next demonstrated that the amplitude of the sperm swing decreased remarkably in the *Tcte1*$^{-/-}$ mice, compared to controls (Fig. 4C). Therefore, the significantly low fertilization rate may be due to poor sperm motility. Based on these data, it was suspected that certain unidentified functional differences between mice and human sperms may have prevented the *Tcte1*$^{-/-}$ micesperm from fertilizing in vitro, whereas, this is easily achieved with humans sperms via IVF.

No obvious hydrocephalus and tracheal ciliary defectswas observed in the *Tcte1* deficient mice

Being an essential component of the sperm flagella and cilia, N-DRCs deficiency is likely to cause primary ciliary dyskinesia (PCD)-related phenotypes, owing to the ciliary defects. We thus investigated whether the PCD-related phenotype exists in the *Tcte1*$^{-/-}$ mice. Upon initial observation, we noticed that the *Tcte1*$^{-/-}$ mice can live to adulthood. Next, immunofluorescent staining and immunoblotting confirmed the absense of TCTE1 in the respiratory tract cilia of *Tcte1*$^{-/-}$ mice (Fig. 5A, B). Further, we compared the brain and trachea of the *Tcte1*$^{-/-}$ mice with wild-type mice. Using H & E staining of the coronal sections of mice brain tissues, we demonstrated that the four ventricles of *Tcte1*$^{-/-}$ mice displayed no significant enlargement, indicating that *Tcte1* deficiency does not produce severe hydrocephalus in mice (Fig. 5C). In addition, analysis of the cilia length suggested that mice TCTE1 deletion did not affect tracheal cilia (Fig. 5D, E). Hence, *Tcte1* deficiency in mice does not induce obvious hydrocephalus and tracheal ciliary defects.

DISCUSSION

Here, we reported a case of AZS in a male patient with low sperm motility and no apparent structural defects. In order to further explore the exact cause of AZS, we conducted genetic testing via WES and detected a two-base insertion between the 396th and 397th bases of the TCTE1 gene coding sequence, which generated an amino acid termination code earlier in the gene sequence. The variant, ENST0000371505.5: c.396_397insTC(p.Arg133Serfs*33), therefore, resulted in a truncated and dysfunctional TCTE1 protein, which lead to infertility.

N-DRC is a highly conserved structural complex located in the axoneme of the cilium and flagellum. Based on the *Chlamydomonas* flagellar study, N-DRC contributes to the oscillation of the flagellum axoneme. In addition, a recent report demonstrated that the DRC1$^{R554X/R554X}$ variant is intricately associated with severe axonemal disorganization and unassembled microtubule doublets [35]. Following examination of the sperm flagellum axoneme structure in our patient, we discovered no obvious abnormality in the axoneme structure, which is similar to the *Tcte1*$^{-/-}$ mice. Unlike the *Drc1* knock-out phenotype, there was no disorder in the "9 + 2" microtubule, as evidenced by TEM. Moreover, the N-DRC complex was still present.

N-DRCs deficiency raises the possibility of PCD-related phenotypes, due to ciliary motility defects. In fact, deficiencies in *DRC1*, *CCDC65/DRC2*, and *GAS8/DRC4* often produce a PCD phenotype [30, 40–45]. In our study, the patient did not show clinical features of PCD other than infertility. Whether *Tcte1*-defects lead to other PCD-related phenotypes requires additional clinical tests, such as nasal nitric oxide measurement, assessment of ciliary waveform by high speed video microscopy [46]. In this study, we evaluated the pathogenicity of TCTE1 deficiency in relation to PCD in a mice model, and no obvious abnormalities were found in the *Tcte1*$^{-/-}$ mice brain and tracheal cilia, relative to wild type mice.

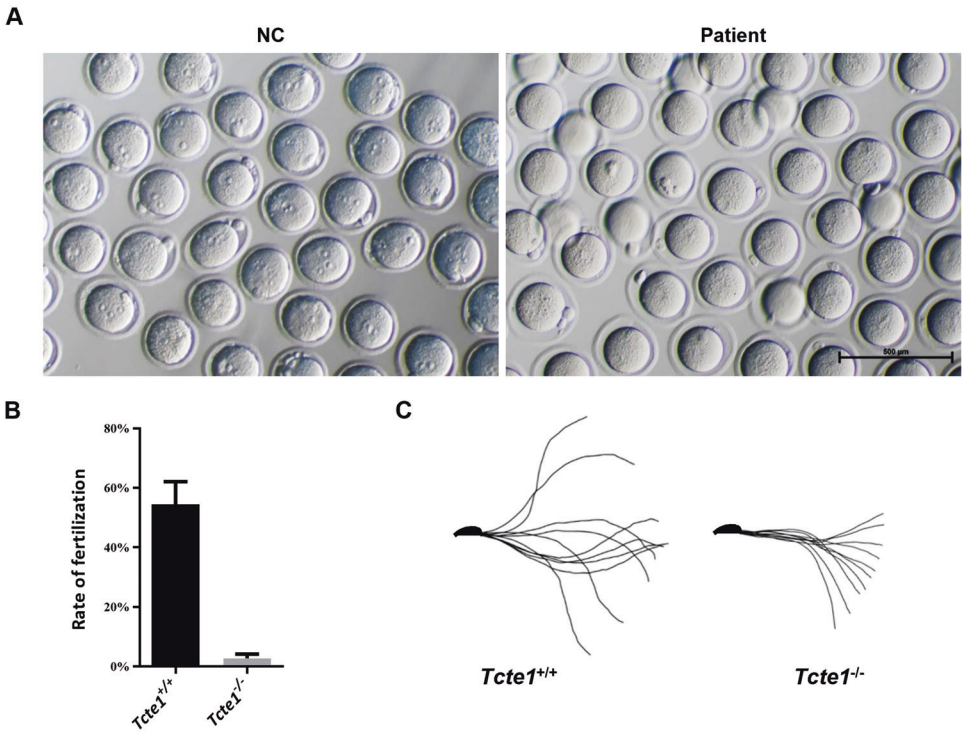

Fig. 4 Mice IVF experiment and movement analysis. A, B Mice IVF assessment. Images of egg fertilization with spermatozoa from wild-type and *Tcte1*$^{-/-}$ mice; scale bar = 500 μm. **A** Column chart depicting the drastically low fertilization rates of *Tcte1*$^{-/-}$ mice, as compared to control mice ($n = 5$) (**B**). **C** The Bohboh analysis software revealing the movement mode of spermatozoa from both wild-type and *Tcte1*$^{-/-}$ mice.

Table 3. IVF data of mice.

Mus	Egg	Zygote	2-cell	4-cell	8-cell	Blastocyst
WT-1	147	70	64	62	62	62
WT-2	140	65	61	61	53	53
WT-3	81	36	36	34	17	14
WT-4	70	34	34	34	26	25
WT-5	80	68	58	42	38	34
Hom-1	156	9	9	5	4	2
Hom-2	178	3	3	1	0	0
Hom-3	127	0	0	0	0	0
Hom-4	62	0	0	0	0	0
Hom-5	78	5	3	0	0	0

In a study examining the *Chlamydomonas* flagella, ~11 proteins (DRC1–11) were attributed to the N-DRC complex. In the N-DRC complex, DRC1/2/4 forms a core complex that behaves as the docking site for "functional subunits" like DRC3/5-8/11 [34]. Hence, being a "functional subunit", TCTE1 loss does not significantly affect assembly of other components. Notably, this structure may vary slightly between species. For example, DRC1 deletion in *Chlamydomonas* results in the complete failure of the N-DRC structural assembly, followed by abnormal motility. However, the basic axoneme structure remained normal. In contrast, DRC1 deletion in mice flagella produced severe axoneme basic structural disorganization (Zhang et al. [35]). Prior evidences suggested that the sperm axoneme structure in *Tcte1*$^{-/-}$ mice remains normal, whereas the normal function of forward sperm motility is lost [27]. In this study, we verified that the TCTE1 loss did not affect expression of DRC1-4/7 protein within the sperm flagella. Additionally, we also observed the same results using immunofluorescence in our AZS patient. Collectively, we demonstrated here, for the first time, that TCTE1 loss in our patient and in mice does not influence assembly of other essential N-DRC components like DRC1-4/7.

It is well known that human and mice oocytes require distinct incubation periods for maturation before fertilization [47, 48]. Hence, incomplete incubation times can lead to markedly different IVF outcomes for both human and mice sperms, with similar AZS phenotype. In our study, we demonstrated that the TCTE1 deficient human sperms had higher fertilization rates, using IVF, than mice sperms. This suggests that the *Tcte1* deficient mice model is likely not a good reference for the assessment of assisted reproductive measures of patients with TCTE1 defects. Furthermore, this difference also suggests that fertilization in the two species may be not equally dependent on sperm motility. Since only one TCTE1-deficient patient was screened, more experiments are needed to confirm our conclusions.

In general, we screened a case of AZS, brought on by a variant in the *TCTE1* gene. Similar to the *Tcte1*$^{-/-}$ mice, the sperm viability

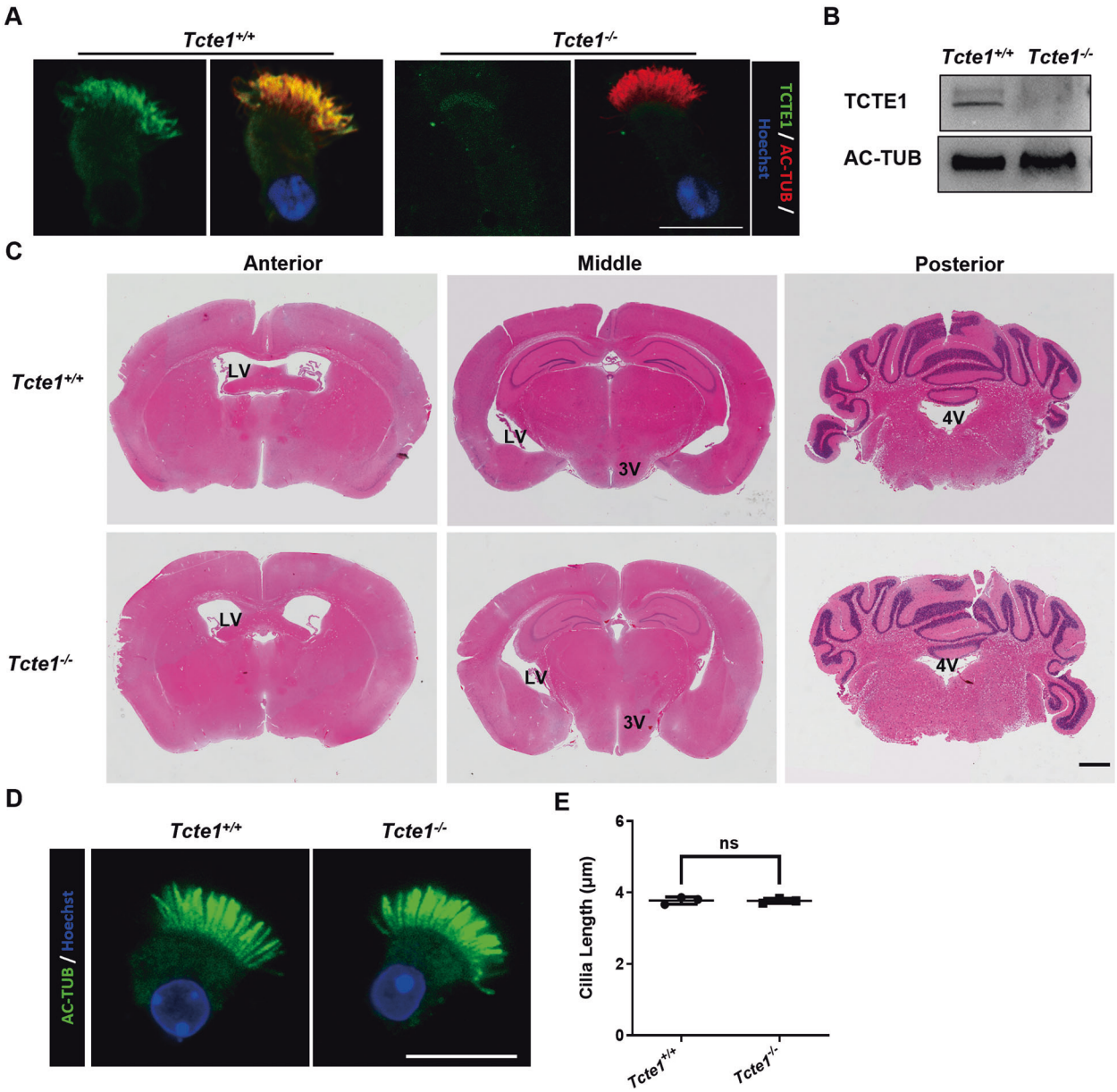

Fig. 5 Morphological observation of brain and tracheal cilia in mice. A The respiratory epithelial cells were dual-stained with an antibody marker specific for the ciliary axoneme (acetylated-tubulin, green) and TCTE1. The TCTE1 could be detected in the *Tcte1*$^{+/+}$ group, while no signal was evident in *Tcte1*$^{-/-}$ samples. **B** TCTE1 expression could be detected in the *Tcte1*$^{+/+}$ respiratory epithelial cells using Western blot. **C** Coronal mice brain sections stained with HE. Lateral ventricles (LV), third ventricles (3 V), and fourth ventricles (4 V) are marked in corresponding positions on the images; scale bar = 1 mm. **D** Immunofluorescent evaluation of acetylated-tubulin (green) and Hoechst (blue) in the tracheal ciliated columnar epithelial cells; scale bar = 10 μm. (**E**) Harvested respiratory cilia length evaluation from wild-type and *Tcte1*$^{-/-}$ mice. Each dot represents the average cilia length of one analyzed specimen ($n = 71$ vs. 68 cells). AC-TUB, acetylated-TUBULIN; ns, no significance.

and forward motility of our patient were significantly abnormal, but there was no obvious abnormality in appearance and morphology. Furthermore, our study showed that TCTE1 is a functional constituent of the DRC complex, and the absence of TCTE1 does not affect assembly of other DRC components. The conclusions in this paper uncover certain mechanistic aspects of the TCTE1 deficient AZS phenotype, which could help to provide a target for the diagnosis of male infertility and suggest that the variation of such gene can be solved by IVF.

DATA AVAILABILITY

The data associated with this article can be shared upon reasonable request.

REFERENCES

1. Curi SM, Ariagno JI, Chenlo PH, Mendeluk GR, Pugliese MN, Sardi Segovia LM, et al. Asthenozoospermia: analysis of a large population. Arch Androl. 2003;49:343–9.
2. Ben Khelifa M, Coutton C, Zouari R, Karaouzene T, Rendu J, Bidart M, et al. Mutations in DNAH1, which encodes an inner arm heavy chain dynein, lead to male infertility from multiple morphological abnormalities of the sperm flagella. Am J Hum Genet. 2014;94:95–104.
3. Coutton C, Martinez G, Kherraf ZE, Amiri-Yekta A, Boguenet M, Saut A, et al. Bi-allelic mutations in ARMC2 lead to severe astheno-teratozoospermia due to sperm flagellum malformations in humans and mice. Am J Hum Genet. 2019;104:331–40.
4. He X, Li W, Wu H, Lv M, Liu W, Liu C, et al. Novel homozygous CFAP69 mutations in humans and mice cause severe asthenoteratospermia with multiple morphological abnormalities of the sperm flagella. J Med Genet. 2019;56:96–103.

5. He X, Liu C, Yang X, Lv M, Ni X, Li Q, et al. Bi-allelic loss-of-function variants in CFAP58 cause flagellar axoneme and mitochondrial sheath defects and asthenoteratozoospermia in humans and mice. Am J Hum Genet. 2020;107:514–26.
6. Liu C, He X, Liu W, Yang S, Wang L, Li W, et al. Bi-allelic mutations in TTC29 Cause Male Subfertility with Asthenoteratospermia in Humans and Mice. Am J Hum Genet. 2019;105:1168–81.
7. Liu C, Miyata H, Gao Y, Sha Y, Tang S, Xu Z, et al. Bi-allelic DNAH8 variants lead to multiple morphological abnormalities of the sperm flagella and primary male infertility. Am J Hum Genet. 2020;107:330–41.
8. Liu W, He X, Yang S, Zouari R, Wang J, Wu H, et al. Bi-allelic mutations in TTC21A induce asthenoteratospermia in humans and mice. Am J Hum Genet. 2019;104:738–48.
9. Liu W, Sha Y, Li Y, Mei L, Lin S, Huang X, et al. Loss-of-function mutations in SPEF2 cause multiple morphological abnormalities of the sperm flagella (MMAF). J Med Genet. 2019;56:678–84.
10. Lorès P, Coutton C, El Khouri E, Stouvenel L, Givelet M, Thomas L, et al. Homozygous missense mutation L673P in adenylate kinase 7 (AK7) leads to primary male infertility and multiple morphological anomalies of the flagella but not to primary ciliary dyskinesia. Hum Mol Genet. 2018;27:1196–211.
11. Lv M, Liu W, Chi W, Ni X, Wang J, Cheng H, et al. Homozygous mutations in DZIP1 can induce asthenoteratospermia with severe MMAF. J Med Genet. 2020;57:445–53.
12. Sha YW, Xu X, Mei LB, Li P, Su ZY, He XQ, et al. A homozygous CEP135 mutation is associated with multiple morphological abnormalities of the sperm flagella (MMAF). Gene. 2017;633:48–53.
13. Shen Y, Zhang F, Li F, Jiang X, Yang Y, Li X, et al. Loss-of-function mutations in QRICH2 cause male infertility with multiple morphological abnormalities of the sperm flagella. Nat. Commun. 2019;10:433.
14. Tang S, Wang X, Li W, Yang X, Li Z, Liu W, et al. Biallelic mutations in CFAP43 and CFAP44 cause male infertility with multiple morphological abnormalities of the sperm flagella. Am J Hum Genet. 2017;100:854–64.
15. Auguste Y, Delague V, Desvignes J-P, Longepied G, Gnisci A, Besnier P, et al. Loss of Calmodulin- and Radial-Spoke-Associated Complex Protein CFAP251 leads to immotile spermatozoa lacking mitochondria and infertility in men. Am J Hum Genet. 2018;103:413–20.
16. Li W, He X, Yang S, Liu C, Wu H, Liu W, et al. Biallelic mutations of CFAP251 cause sperm flagellar defects and human male infertility. J Hum Genet. 2019;64:49–54.
17. Liu S, Zhang J, Kherraf ZE, Sun S, Zhang X, Cazin C, et al.: CFAP61 is required for sperm flagellum formation and male fertility in human and mouse. bioRxiv 2021: 2021.2003.2004.433881.
18. Tu C, Wang W, Hu T, Lu G, Lin G, Tan YQ. Genetic underpinnings of asthenozoospermia. Best Pract Res Clin Endocrinol Metab. 2020;34:101472.
19. Wilton LJ, Temple-Smith PD, de Kretser DM. Quantitative ultrastructural analysis of sperm tails reveals flagellar defects associated with persistent asthenozoospermia. Hum Reprod. 1992;7:510–6.
20. Xu X, Sha YW, Mei LB, Ji ZY, Qiu PP, Ji H, et al. A familial study of twins with severe asthenozoospermia identified a homozygous SPAG17 mutation by whole-exome sequencing. Clin Genet. 2018;93:345–9.
21. Olbrich H, Häffner K, Kispert A, Völkel A, Volz A, Sasmaz G, et al. Mutations in DNAH5 cause primary ciliary dyskinesia and randomization of left-right asymmetry. Nat Genet. 2002;30:143–4.
22. Antony D, Becker-Heck A, Zariwala MA, Schmidts M, Onoufriadis A, Forouhan M, et al. Mutations in CCDC39 and CCDC40 are the major cause of primary ciliary dyskinesia with axonemal disorganization and absent inner dynein arms. Hum Mutat. 2013;34:462–72.
23. Castleman VH, Romio L, Chodhari R, Hirst RA, de Castro SC, Parker KA, et al. Mutations in radial spoke head protein genes RSPH9 and RSPH4A cause primary ciliary dyskinesia with central-microtubular-pair abnormalities. Am J Hum Genet. 2009;84:197–209.
24. Moye AR, Bedoni N, Cunningham JG. Mutations in ARL2BP, a protein required for ciliary microtubule structure, cause syndromic male infertility in humans and mice. PLoS Genet. 2019;15:e1008315.
25. Heuser T, Raytchev M, Krell J, Porter ME, Nicastro D. The dynein regulatory complex is the nexin link and a major regulatory node in cilia and flagella. J cell Biol. 2009;187:921–33.
26. Bower R, Tritschler D, Vanderwaal K, Perrone CA, Mueller J, Fox L, et al. The N-DRC forms a conserved biochemical complex that maintains outer doublet alignment and limits microtubule sliding in motile axonemes. Mol Biol cell. 2013;24:1134–52.
27. Castaneda JM, Hua R, Miyata H, Oji A, Guo Y, Cheng Y, et al. TCTE1 is a conserved component of the dynein regulatory complex and is required for motility and metabolism in mouse spermatozoa. Proc Natl Acad Sci USA. 2017;114: E5370–78.
28. Liu M, Shi X, Bi Y, Qi L, Guo X, Wang L, et al. SHCBP1L, a conserved protein in mammals, is predominantly expressed in male germ cells and maintains spindle stability during meiosis in testis. Mol Hum Reprod. 2014;20:463–75.
29. Hasuwa H, Muro Y, Ikawa M, Kato N, Tsujimoto Y, Okabe M. Transgenic mouse sperm that have green acrosome and red mitochondria allow visualization of sperm and their acrosome reaction in vivo. Exp Anim. 2010;59:105–7.
30. Wirschell M, Olbrich H, Werner C, Tritschler D, Bower R, Sale WS, et al. The nexin-dynein regulatory complex subunit DRC1 is essential for motile cilia function in algae and humans. Nat Genet. 2013;45:262–8.
31. Akhmanova A, Mausset-Bonnefont A, van Cappellen W, Keijzer N, Hoogenraad C, Stepanova T, et al. The microtubule plus-end-tracking protein CLIP-170 associates with the spermatid manchette and is essential for spermatogenesis. Genes Dev. 2005;19:2501–15.
32. Oda T, Yanagisawa H, Kikkawa M. Detailed structural and biochemical characterization of the nexin-dynein regulatory complex. Mol Biol cell. 2015;26:294–304.
33. Lin J, Tritschler D, Song K, Barber CF, Cobb JS, Porter ME, et al. Building blocks of the nexin-dynein regulatory complex in Chlamydomonas flagella. J Biol Chem. 2011;286:29175–91.
34. Gui L, Song K, Tritschler D, Bower R, Yan S, Dai A, et al. Scaffold subunits support associated subunit assembly in the Chlamydomonas ciliary nexin-dynein regulatory complex. Proc Natl Acad Sci USA. 2019;116:23152–62.
35. Zhang J, He X, Wu H, Zhang X, Yang S, Liu C, et al. Loss of DRC1 function leads to multiple morphological abnormalities of the sperm flagella and male infertility in human and mouse. Hum Mol Genet. 2021;30:1996–2011.
36. Bower R, Tritschler D, Mills KV, Heuser T, Nicastro D, Porter ME. DRC2/CCDC65 is a central hub for assembly of the nexin-dynein regulatory complex and other regulators of ciliary and flagellar motility. Mol Biol Cell. 2018;29:137–53.
37. Huang B, Ramanis Z, Luck DJ. Suppressor mutations in Chlamydomonas reveal a regulatory mechanism for Flagellar function. Cell. 1982;28:115–24.
38. Gardner LC, O'Toole E, Perrone CA, Giddings T, Porter ME. Components of a "dynein regulatory complex" are located at the junction between the radial spokes and the dynein arms in Chlamydomonas flagella. J Cell Biol. 1994;127:1311–25.
39. Miyata H, Satouh Y, Mashiko D, Muto M, Nozawa K, Shiba K, et al. Sperm calcineurin inhibition prevents mouse fertility with implications for male contraceptive. Science. 2015;350:442–5.
40. Horani A, Brody SL, Ferkol TW, Shoseyov D, Wasserman MG, Ta-shma A, et al. CCDC65 mutation causes primary ciliary dyskinesia with normal ultrastructure and hyperkinetic cilia. PloS One. 2013;8:e72299.
41. Austin-Tse C, Halbritter J, Zariwala MA, Gilberti RM, Gee HY, Hellman N, et al. Zebrafish ciliopathy screen plus human mutational analysis identifies C21orf59 and CCDC65 defects as causing primary ciliary dyskinesia. Am J Hum Genet. 2013;93:672–86.
42. Olbrich H, Cremers C, Loges NT, Werner C, Nielsen KG, Marthin JK, et al. Loss-of-Function GAS8 mutations cause primary ciliary dyskinesia and disrupt the nexin-dynein regulatory complex. Am J Hum Genet. 2015;97:546–54.
43. Ha S, Lindsay AM, Timms AE, Beier DR. Mutations in Dnaaf1 and Lrrc48 cause hydrocephalus, laterality defects, and sinusitis in mice. G3 (Bethesda). 2016;6:2479–87.
44. Jeanson L, Thomas L, Copin B, Coste A, Sermet-Gaudelus I, Dastot-Le Moal F, et al. Mutations in GAS8, a gene encoding a nexin-dynein regulatory complex subunit, cause primary ciliary dyskinesia with axonemal disorganization. Hum Mutat. 2016;37:776–85.
45. Lewis WR, Malarkey EB, Tritschler D, Bower R, Pasek RC, Porath JD et al. Mutation of growth arrest specific 8 reveals a role in motile cilia function and human disease. PLoS Genet. 2016;12:e1006220.
46. Shoemark A, Boon M, Brochhausen C, Bukowy-Bieryllo Z, De Santi MM, Goggin P et al. International consensus guideline for reporting transmission electron microscopy results in the diagnosis of primary ciliary dyskinesia (BEAT PCD TEM Criteria). Eur Respir J. 2020;55:1900725.
47. Edwards RG. Maturation in vitro of mouse, sheep, cow, pig, rhesus monkey and human ovarian oocytes. Nature. 1965;208:349–51.
48. Ménézo YJ, Hérubel F. Mouse and bovine models for human IVF. Reprod Biomed Online. 2002;4:170–5.

ACKNOWLEDGEMENTS

We extend our appreciation to Fan Hu and Jinyang Cai for their support and provision of the microscope.

FUNDING

This work was supported by the Natural Science Foundation of China (31771654 and 32070842 to ML, 32000584 to RH, 82171607 to XH, 81901541 to HW); the Non-profit Central Research Institute Fund of the Chinese Academy of Medical Sciences (Grant

no. 2019PT310002 to YC); the Natural Science Foundation of Jiangsu Province (Grants No. BK20190081 to ML); the Science and Technology Project of Anhui Province (Grant No.202003a07020012 to PZ); and Qing Lan Project (to ML).

COMPETING INTERESTS

The authors declare no competing interests.

ETHICAL APPROVAL

Clinical exome sequencing was approved by the ethics committees of the First Affiliated Hospital of Anhui Medical University, Number P2020-12-36. All human subjects provided informed consent for this study.

ADDITIONAL INFORMATION

Supplementary information The online version contains supplementary material available at https://doi.org/10.1038/s41431-022-01095-w.

Correspondence and requests for materials should be addressed to Rong Hua, Yunxia Cao or Mingxi Liu.